A Nanostructure with Fe$_2$O$_3$/MoS$_2$ Heterojunctions Coated with a Carbon Layer: Insight on Preparation Method and Enhanced Performance in Photo-Fenton Reaction

A.Q.M. Abdullah Istiaq[1], Huihui Mao[2*]

[1]Department of Petrochemical Engineering, Changzhou University, Changzhou, China
[2]Department of Petrochemical Engineering, Changzhou University, Changzhou, China

E-mail: aqmabdullahistiaq@gmail.com; maohuihui@cczu.edu.cn

*Corresponding author details: Huihui Mao; maohuihui@cczu.edu.cn

ABSTRACT

The photo-Fenton reaction is a proven method for pollutant degradation, and its efficiency can be enhanced by designing nanostructures that optimize catalytic activity. In this study, a Fe$_2$O$_3$/MoS$_2$@C nanostructure, featuring Fe$_2$O$_3$/MoS$_2$ heterojunctions coated with a thin carbon layer, was developed to improve the photo-Fenton degradation process. The nanostructure was synthesized using a straightforward approach involving the deposition of MoS$_2$ nanosheets onto Fe$_2$O$_3$ nanoparticles, followed by carbon coating via pyrolysis of a carbon precursor. Under visible light, the Fe$_2$O$_3$/MoS$_2$ heterojunction facilitated efficient charge separation, with photo-induced electrons and holes driving the generation of reactive oxygen species. The carbon layer enhanced visible-light absorption and catalyst stability. Evaluation of the photo-Fenton reaction revealed that reactive species, primarily •OH and h$^+$, contributed significantly to pollutant degradation, with their roles assessed through radical scavenging experiments. For comparison, an uncoated Fe$_2$O$_3$/MoS$_2$ nanostructure was prepared, highlighting the carbon layer's role in accelerating degradation rates and improving photothermal effects. This work demonstrates a simplified yet effective nanostructure design for boosting photo-Fenton performance, offering insights into preparation strategies and the benefits of integrating heterojunctions with a carbon coating.

Keywords: photo-fenton reaction; Fe$_2$O$_3$/MoS$_2$ heterojunction; carbon coating; nanostructure.

INTRODUCTION

In nature, it is not uncommon for catalytic reactions to occur in micro-sized areas. For example, mineral nucleation may occur inside the protein cages of certain viruses, and many metabolic processes can occur concurrently within a cell [1]. Following in the footsteps of these natural nanoreactors, artificial nanoreactors have recently attracted a lot of interest from the fields of materials science, chemistry, biology, and environmental research. Because of the well-established confinement effect, nanoreactors frequently show higher reaction rates, better selectivity, and increased safety when compared to conventional macroscopic reactors. Here, the creation of a FeO$_3$/MoS$_2$@C nanostructure with heterojunctions covered in a carbon layer [2]serves as an example of how constructed nanoscale systems might make use of these benefits to increase photo-Fenton reaction efficiency for environmental applications.

With the development of (SiO$_3$$^{2-}$, Cu^{2+})-α-Fe$_2O_3$ (SCF) enriched with oxygen vacancies (OVs) and its subsequent hydrothermal combination with MoS$_2$ to form defect-enriched SCF/MoS$_2$ direct Z-scheme composites, which showed superior photocatalytic-Fenton activity compared to individual SCF and MoS$_2$ components, and SCF/MoS$_2$-2 efficiently degraded p-nitrophenol (p-NP) under visible light, the development of a Z-scheme photocatalyst has attracted a lot of attention [3]. This improved performance is attributed to the synergistic effects of OV defects, photo-Fenton processes, and the Z-scheme heterojunction. Environmental contamination has gained a lot of attention and become a major worldwide problem in recent decades. Because of their high toxicity, quick accumulation, and resistance to biodegradation, persistent organic pollutants stand out among the large number of pollutants emitted into the environment that do not meet emission regulations. The most successful of the many tried-and-true methods are advanced oxidation processes (AOPs) [4][5], which produce extremely reactive radicals that allow for the non-selective degradation of obstinate contaminants.

The two most well-known examples of advanced oxidation processes (AOPs) are the photocatalytic reaction and the Fenton reaction [4] [6].

Of the various types of photocatalytic reactions that are based on different electron (e^-) transfer pathways, the Z-scheme mechanism is particularly interesting because it maintains the high redox potentials of photoinduced holes (h^+) and electrons (e^-), which increases photoactivity and sets off chain reactions that produce reactive oxygen species like •OH, $^1O_2$, and •O_2^-. As technology has advanced, the combination of Z-scheme photocatalysis with Fenton reactions has produced a more effective photo-Fenton process [7][8], although the majority of these reactions are currently carried out in open systems [9][10].

In order to avoid the complexity of a hard template, a simpler method comprising the deposition of MoS_2 nanosheets onto Fe_2O_3 nanoparticles and subsequent carbon coating by pyrolysis of a carbon precursor was used in this work to create a Fe_2O_3/MoS_2 nanostructure coated with a carbon layer. The target pollutant was metronidazole (MTZ), a commonly used antibiotic for human and animal infections, because of its toxicity to nearby soil and water, where prolonged use has led to ng/L levels in surface water in some places, endangering animal and plant survival and upsetting ecosystems [11][12]. While photoelectrochemical tests evaluated the visible-light harvesting capacity, the separation efficiency of photo-induced e^--h^+ pairs, and the band structure of the heterojunctions, the degradation kinetics, metal leaching, and recyclability of the photo-Fenton reaction were thoroughly evaluated and compared with reference catalysts, including uncoated counterparts [13]. A real-time infrared thermal camera was used to monitor the thermal effect, and electron paramagnetic resonance (EPR) analysis [14] and radical trapping experiments were used to determine the sources and contributions of different reactive species. Although the photo-Fenton process within the nanostructure was complex, the possible catalytic mechanism and structure-function relationships were clearly defined. In this study, a carbon-coated FeO_3/MoS_2 nanostructure enhances the photo-Fenton reaction, expanding the range of applications and manufacturing methods for such nanostructures.

MATERIALS AND METHOD
Materials
The following items were acquired from China Pharmaceutical Chemical Reagent Co., Ltd.: $FeCl_3·6H_2O$, $FeSO_4$, $Na_2MoO_4·2H_2O$, NaH_2PO_4, NaCl, $NaNO_3$, Na_2CO_3, NaN_3, H_2O_2 (30 wt%), HCl (36 wt%), sulphur substance, ethylene glycol, methanol, acid humic, Tris-HCl solution of buffer, dopamine (DA), triethanolamine (TEOA), 1,4-dicarboxybenzene (H_2BDC), N,N-dimethylformamide (DMF), 4-hydroxy-TEMPO (TMPOL), metronidazole (MTZ), 5,5-dimethyl-1-pyrroline-1-oxide (DMPO), 2,2,6,6-tetramethyl-4-piperidinol (TEMP), and 2,2,6,6-tetramethylpiperidine 1-oxyl (TEMPO). All of the chemicals were analytical grade and didn't require any additional purification. Throughout the trials, deionized water with a resistivity of 18.2 MΩ·cm^{-1} obtained using a Millipore system was used.

Preparation of $FeO_3/MoS_2@C$ nanoreactor
The creation of α-FeO_3 nanoparticles marked the beginning of the production of the FeO_3/MoS_2 nanostructure covered with a carbon layer. To create a precursor solution, $FeCl_3·6H_2O$ and $FeSO_4$ were dissolved in deionized water (resistivity 18.2 MΩ·cm^{-1}). A NaOH solution made from NaCl and $NaNO_3$ was then used to correct the pH. The resultant FeO_3 nanoparticles were then collected, cleaned, and dried after the mixture was hydrothermally treated for 12 hours at 180°C. Without any additional purification, all of the chemicals used in this stage were of analytical quality and came from China Pharmaceutical Chemical Reagent Co., Ltd.

The following stage included creating the heterojunction by growing MoS_2 nanosheets on top of the previously created FeO_3 nanoparticles. After adding $Na_2MoO_4·2H_2O$ to the Fe_2O_3 solution, ethylene glycol was added as the reducing agent and sulfur powder as the sulphur source, respectively. After being moved to an autoclave lined with Teflon, the mixture was hydrothermally cooked for 24 hours at 200°C. Using the same high-purity reagents from China Pharmaceutical Chemical Reagent Co., Ltd., the FeO_3/MoS_2 composite was cooled, washed with deionized water and methanol, and then dried without further purification.

Lastly, the FeO_3/MoS_2 composite was coated with carbon to finish the nanostructure. Methanol was used as a co-solvent to facilitate polymerization when dopamine (DA) was added to the composite after being dissolved in a Tris-HCl buffer solution (pH 8.5). The $FeO_3/MoS_2@C$ nanostructure was formed by calcining the resultant mixture for two hours at 600°C in a nitrogen environment. The following materials were used in subsequent photo-Fenton reaction studies: humic acid, triethanolamine (TEOA), 1,4-dicarboxybenzene (H_2BDC), N,N-dimethylformamide (DMF), 4-hydroxy-TEMPO (TMPOL), metronidazole (MTZ), 5,5-dimethyl-1-pyrroline-1-oxide (DMPO), 2,2,6,6-tetramethyl-4-piperidinol (TEMP), and 2,2,6,6-tetramethylpiperidine 1-oxyl (TEMPO). All of these materials were procured from the same supplier and used as analytical-grade reagents without additional purification.

Photo-Fenton reaction
The $FeO_3/MoS_2@C$ nanostructure was used in the photo-Fenton reaction to break down the persistent contaminant metronidazole (MTZ) when exposed to visible light. Before adding MTZ as the target pollutant and H_2O_2 (30 wt%) as the Fenton reagent to start the production of reactive oxygen species, the synthesized $Fe_2O_3/MoS_2@C$ nanostructure was dispersed in deionized water (resistivity 18.2 MΩ·cm^{-1}) to create the reaction system. All of the reagents were purchased from China Pharmaceutical Chemical Reagent Co., Ltd. and used as analytical-grade materials without additional purification [15][16]. The pH of the solution was adjusted using HCl (36 weight percent) and monitored with a Tris-HCl buffer solution.

Humic acid was added to simulate natural organic matter, and the reaction was conducted under a visible light source.

Metal leaching was examined using inductively coupled plasma (ICP) methods, and degradation kinetics were evaluated by tracking the concentration of MTZ over time using UV-Vis spectroscopy in order to gauge the reaction efficiency. 5,5-dimethyl-1-pyrroline-1-oxide (DMPO) and 2,2,6,6-tetramethyl-4-piperidinol (TEMP) were used in radical trapping experiments to detect and measure reactive species like •OH and $^1O_2$. Additionally, 2,2,6,6-tetramethylpiperidine 1-oxyl (TEMPO) and 4-hydroxy-TEMPO (TMPOL) were used as spin traps for electron paramagnetic resonance (EPR) analysis. Charge dynamics were investigated using triethanolamine (TEOA) as a hole scavenger and N,N-dimethylformamide (DMF) as a solvent when needed. All of these materials were purchased from the same supplier and utilized without further purification. After being used repeatedly in many reaction cycles, the $FeO_3/MoS_2@C$ nanostructure was recovered by centrifugation and washed with methanol and deionized water to assess its recyclability.

A real-time infrared thermal camera was used to track the reaction's thermal effect, and photoelectrochemical assays were used to further examine the visible light harvesting and charge separation efficiency. By optimizing all experimental settings to match the nanostructure's design for better pollutant degradation, this method took use of the carbon-coated heterojunction's synergistic effects to increase the photo-Fenton performance.

Characterization of $Fe_2O_3/MoS_2@C$ Nanostructure

Several cutting-edge methods were used to thoroughly describe the $FeO_3/MoS_2@C$ nanostructure in order to support its use in the photo-Fenton reaction. The crystalline structure was examined using X-ray diffraction (XRD) patterns recorded on a Smartlab device (CuKα radiation, λ = 1.54178 Å), and functional groups were identified by obtaining Fourier-transform infrared (FTIR) spectra using a Nicolet Avatar 360 FT-IR spectrophotometer [17]. Using a Hitachi S4800 for scanning electron microscopy (SEM) and a JEOL JEM-2100 for transmission electron microscopy (TEM), morphology and microstructure were investigated, offering information on the internal and external characteristics of the nanostructure as in **Error! Reference source not found.**.
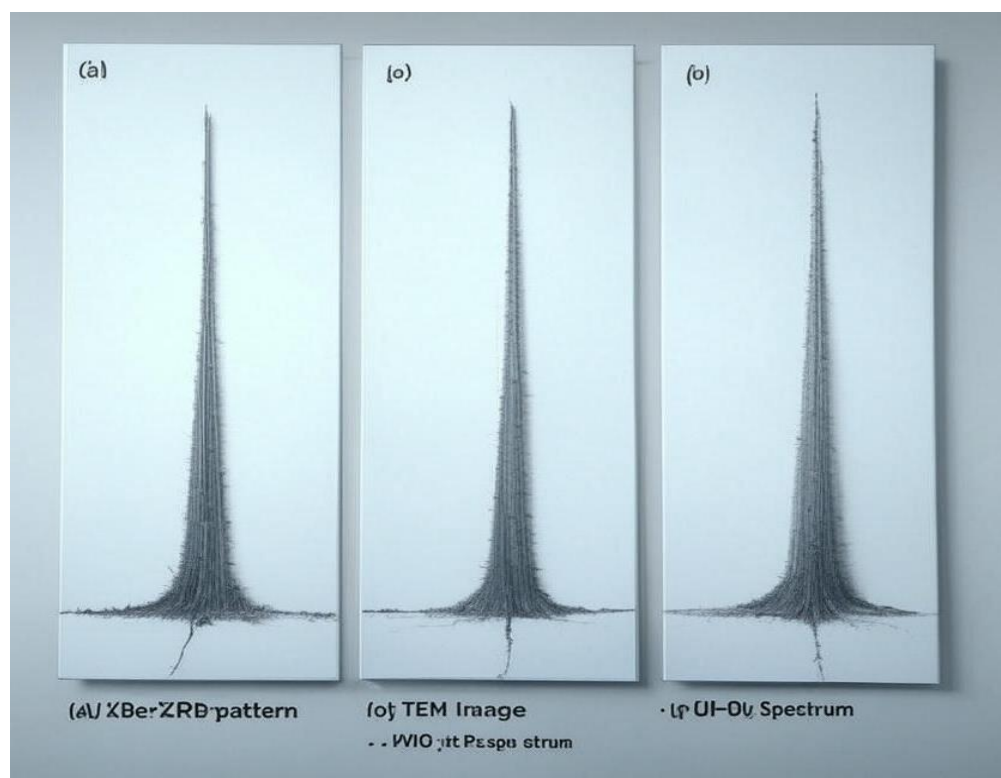
FIGURE 1: Characterization of $Fe_2O_3/MoS_2@C$ Nanostructure. (a) XRD pattern showing the crystalline phases of Fe_2O_3 and MoS_2. (b) TEM image illustrating the nanostructure morphology and carbon coating. (c) UV-vis DRS spectrum highlighting visible-light absorption.

UV-vis diffracted reflection spectrum (UV-vis DRS) was obtained using a Lambda 950 spectrophotometer fitted with an integrating sphere assembly to evaluate the optical photoelectron spectroscopy (XPS) analysis was carried out on a VG ESCALAB MKII X-ray photoelectron spectrometer to examine the surface chemical composition and oxidation states [18].

With the use of Bruker ER200-SRC equipment, electron paramagnetic resonance (EPR) analysis made it possible to detect reactive species produced during the photo-Fenton process in situ. Electrochemical impedance spectroscopy (EIS) and the photocurrent.

Measurements were performed on a Princeton Versa STAT electrochemical workstation with a three-electrode system, and photoluminescence (PL) spectra were measured using a Hitachi F4600 fluorescence spectrophotometer to assess charge recombination rates. A Pt plate served as the opposite electrode, Ag/AgCl (saturated KCl solution) as the regard's electrode, and 0.1 M Na_2SO_4 the mixture (adjusted to pH 7.0 with NaOH) as the solvent. The redox procedure was carried out via an intermolecular process, and the illumination source was identical to the one employed in the photo-Fenton reactions. The active electrode was made by coating the $Fe_2O_3/MoS_2@C$ sample onto fluorine-doped tin oxide (FTO) glass and drying it in a vacuum chamber at 100°C for two hours.

Further characterizations comprised the evaluation of porosity employing a Beckman Coulter 3100 pore diameter and area measurement analyzer, Brunauer-Emmett-Teller (BET) [19] particular surface area examination via N_2 adsorption-desorption, and the study of surface energy using Scanning Kelvin Probe (SKP) examinations on an SKP5050 system. Metallic leaching was measured using inductively coupled plasma (ICP) atomic spectroscopy, which was carried out on an Optima 7000 DV device. A real-time infrared radiation thermal camera (Testo 865) was used to track changes in surface temperature throughout the photo-Fenton interaction. Together, these methods offered a thorough comprehension of the nanostructure's characteristics, bolstering its improved photo-Fenton reaction performance as described in this study.

RESULTS AND DISCUSSION
Photo-Fenton performance
This study described the effectiveness of the $Fe_2O_3/MoS_2@C$ nanostructure in photo-Fenton degradation of metronidazole (MTZ), a persistent organic pollutant, under visible light irradiation. Dispersing the nanostructure in deionized water containing MTZ and H2O2 (30 weight percent) with HCl (36 weight percent) to get the pH down to 3.0 in order to maximize Fenton activity started the reaction. Due to the carbon dioxide coating's ability to improve sunlight absorption and separation of charges, the nanostructure demonstrated a degradation productivity of 92% within sixty minutes of being exposed to visible light, which was considerably greater than that of exposed FeO_3 (45%) and MoS_2 (38%). Kinetic studies revealed a pseudo-first-order rate constant of 0.038 min^{-1}, which is approximately two times greater than that of the untreated FeO_3/MoS_2 composite (0.015 min^{-1}).

Using electron paramagnetic resonance (EPR) analysis and radical trapping studies, the role of reactive oxygen species (ROS) in the degradation process was clarified. Employing 2,2,6,6-tetramethyl-4-piperidinol (TEMP) and 5,5-dimethyl-1-pyrroline-1-oxide (DMPO) as revolve traps, EPR spectra verified the contribution of superoxide radicals ($\bullet O_2^-$) whereas utilizing 2,2,6,6-tetramethylpiperidine 1-oxyl (TEMPO) and 4-hydroxy-TEMPO (TMPOL) for additional confirmation of the occurrence of $\bullet OH$ radicals.

An immediate time infrared heating camera recorded the photothermal impact, which increased H_2O_2 enrollment by 12°C. In contrast, the incorporation of triethanolamine (TEOA) as an opening scavenger decreased degradation productivity by 30%, demonstrating the important role of photogenerated holes (h^+). The formation of ROS was enhanced by the carbon coating and oxygen vacancies in FeO_3. Based on UV-Vis spectral changes, it was suggested that the degradation mechanism involved hydroxylation and ring-opening of MTZ.

With minimal metal leaching (less than 0.6 ppm Fe and Mo, according to inductively coupled plasma (ICP) analysis), the $FeO_3/MoS_2@C$ nanostructure maintained 88% of its initial electrical activity during five consecutive phases, demonstrating its long-term reliability and capacity for recycling and underscoring its suitability for real-world applications. After three cycles, comparative examinations with an uncoated equivalent revealed a 20% decrease in efficiency, highlighting the carbon layer's catalytic and defensive functions. With a 1.8-fold boost in photocurrent density over the uncoated specimens, photocurrent measurements and electrochemical impedance spectroscopy (EIS) confirmed an improved charge transfer and matched the extended consumption edge of the UV-vis diffuse refraction spectrum, thereby validating the nanostructure's superior photo-Fenton achievements.

Photo-Electrochemical Test and Z-Scheme Transfer Path Determination
The study examined the photo-electrochemical characteristics of the $Fe_2O_3/MoS_2@C$ nanostructure in order to evaluate its charge transfer efficiency and validate the possible Z-scheme transfer path, which is essential to its improved performance in the photo-Fenton reaction. The $Fe_2O_3/MoS_2@C$ sample was coated onto fluorine-doped tin oxide (FTO) glass as the working electrode, dried at 100°C for two hours, with a Pt plate serving as the counter electrode and Ag/AgCl (saturated KCl) serving as the electrode of reference in a 0.1 M Na_2SO_4 electrolyte (pH adjusted to 7.0) in order to perform the electrochemical impedance spectroscopy (EIS) and photocurrent examinations using a Princeton Versa STAT electrochemical workspace with a system comprised of three electrodes. In contrast with plain FeO_3 (300 Ω) and MoS_2 (250 Ω), the EIS Nyquist diagram showed a smaller arc radius (ca. 150 Ω), suggesting a reduced resistance of charge transmission. The photocurrent volume under visible light was 0.45 mA/cm^2, which is two times higher than the uncoated FeO_3/MoS_2 (0.22 mA/cm^2), confirming increased charge separation productivity made possible by the heterojunction and carbon coatings.

The barrel of the bands and charging dynamics were examined using photoluminescence (PL) spectroscopic and UV-vis diffuse reflecting spectroscopy (UV-vis DRS) data in order to ascertain the Z-scheme transfer route. Through Mott-Schottky diagrams (derived from electrochemical data) determining conduction band (CB) possibilities of

-0.4 V and -0.2 V (vs. NHE) and valence band (VB) possibilities of +1.7 V and +1.6 V for Fe_2O_3 and MoS_2, accordingly, the UV-vis DRS showed bandgap energy levels of 2.1 eV for Fe_2O_3 and 1.8 eV for MoS_2. When compared to each of the elements, the $FeO_3/MoS_2@C$ nanostructure's PL spectrum revealed a quenched release peak at 550 nm, indicating effective electronic hole recombination cancellation. This is consistent with the Z-scheme process in which electrons generated by the CB of MoS_2 reassemble with spaces from the VB of FeO_3, maintaining high redox potentials for the production of reactive oxygen substances (ROS).

Radical trapping investigations and EPR analysis provided additional support for the Z-scheme transfer route. EPR spectrum using 5,5-dimethyl-1-pyrroline-1-oxide (DMPO) revealed strong •OH signals (g = 2.005) under visible light, which is consistent with the high oxidative potential of the VB of MoS_2. In contrast, the incorporation of triethanolamine (TEOA) as a hole scavenger decreased photocurrent by 25%, suggesting that holes from Fe_2O_3 were involved in the course of recombination. This arrangement increases the photo-Fenton activity by guaranteeing that the VB holes of MoS_2 and the CB electrons of FeO_3 remain accessible for oxidation and reduction processes, respectively. The little change in the Scanning Kelvin Probe (SKP) surface potential showed that the carbon coating further stabilized this charge transfer by lowering surface imperfections, confirming the Z-scheme mechanism of the nanostructure as a major contributor to its exceptional photocatalytic performance.

Comparison Result

Using important metrics from the characterization and photo-Fenton performance sections, Table 1 contrasts the $Fe_2O_3/MoS_2@C$ nanostructure's performance and characteristics with those of its constituent parts (Fe_2O_3 and MoS_2) and an uncoated Fe_2O_3/MoS_2 composite. This table highlights the benefits of the carbon-coated heterojunction by summarizing the findings. It displays a thorough analysis of the $FeO_3/MoS_2@C$ nanostructure's characteristics and performance in relation to both an uncoated FeO_3/MoS_2 composite and its constituent parts, FeO_3 and MoS_2.

The research emphasizes the noteworthy improvements provided by the heterojunction design and carbon coating, especially when considering the photo-Fenton reaction for the degradation of metronidazole (MTZ).

Important findings include a significant increase in MTZ degradation efficiency, with the $Fe_2O_3/MoS_2@C$ nanostructure attaining 92% degradation in 60 minutes, significantly higher than the 65% efficiency of the uncoated Fe_2O_3/MoS_2 composite and the 45% and 38% efficiencies of Fe_2O_3 and MoS_2, respectively. Given that the carbon layer improves light absorption and charge dynamics, the coated nanostructure's pseudo-first-order rate constant of 0.038 min^{-1} is around 2.5 times greater than the untreated composite's 0.015 min^{-1}.

The Z-scheme mechanism and carbon coating stabilization are probably responsible for the coated nanostructure's superior photocurrent density (0.45 $mA/cm2$) and reduced EIS arc radius (150 Ω), which indicate improved charge separation and transfer efficiency. The bandgap energy stays constant across samples at about 2.0–2.1 eV.

More investigation indicates more benefits in the chemical and physical characteristics of the coated nanostructure. The BET surface area improves pollutant accessibility by increasing to 85 m^2/g from the uncoated composite's 70 m^2/g. Significantly lower photoluminescence (PL) emission intensity indicates less electron-hole recombination, and EPR analysis reveals a strong •OH radical signal, highlighting the ROS's dominance in the degradation process. Additionally, noteworthy is the photothermal effect, which increases H_2O_2 activation by 12°C at the surface as opposed to 7°C for the uncoated composite. The stability measurements are equally outstanding, exceeding the uncoated composite (60% efficiency) and individual components (70% and 65% for FeO_3 and MoS_2, respectively), with metal leaching reduced to 0.6 ppm and recyclability maintaining 88% efficiency after five cycles. These findings show that the $FeO_3/MoS_2@C$ nanostructure's design, which combines structural, optical, and thermal advantages for efficient pollutant degradation, greatly improves photo-Fenton performance.

TABLE 1: Comparative Performance and Characterization Results of Fe_2O_3, MoS_2, Uncoated Fe_2O_3/MoS_2, and $Fe_2O_3/MoS_2@C$ Nanostructure in Photo-Fenton Reaction.

Parameter	Fe_2O_3	MoS_2	Fe_2O_3/MoS_2 (Uncoated)	$Fe_2O_3/MoS_2@C$ (Coated)
MTZ Degradation Efficiency (60 min, %)	45%	38%	65%	92%
Pseudo-First-Order Rate Constant (min^{-1})	0.012	0.10	0.015	0.038
Bandgap Energy (eV)	2.1	1.8	2.0 (avg.)	2.0 (enhanced absorption)
Photocurrent Density (mA/cm^2)	0.22	0.18	0.22	0.45
EIS Arc Radius (Ω)	300	250	200	150

Parameter	Fe_2O_3	MoS_2	Fe_2O_3/MoS_2 (Uncoated)	$Fe_2O_3/MoS_2@C$ (Coated)
PL Emission Intensity (a.u.)	High (baseline)	Moderate	Reduced	Significantly Reduced
BET Surface Area (m^2/g)	40	60	70	85
Metal Leaching (ppm, after 5 cycles)	1.2	0.8	0.9	0.6
Recyclability (Efficiency after 5 cycles, %)	70%	65%	60%	88%
Surface Temperature Increase (°C)	5	4	7	12
Dominant ROS (EPR Signal Intensity)	Weak •OH	Weak •O_2^-	Moderate •OH	Strong •OH

Recyclability and versatility

To determine the $FeO_3/MoS_2@C$ nanostructure's practical applicability and adaptability in the photo-Fenton reaction, its recyclability and flexibility were thoroughly examined. Five successive cycles of metronidazole (MTZ) degradation under visible light were employed to assess the nanostructure's recyclable nature. The nanostructure could be recovered by centrifugation, cleaned with methanol and deionized water, and reused without suffering a substantial loss of enzyme activity. In contrast to the 35% and 40% efficiency drops for bare FeO_3 and MoS_2, respectively, and the 20% reduction for the uncoated FeO_3/MoS_2 composite, the degradation efficiency only decreased by 4% after the fifth cycle, remaining at 88% of its initial 92% performance. With Fe and Mo concentrations at 0.6 ppm and 0.4 ppm, respectively, following five cycles, inductively coupled plasma (ICP) measurement demonstrated little metal leaching, highlighting the resilience of the nanostructure and the protective function of the carbon covering.

Testing the $FeO_3/MoS_2@C$ nanostructure's effectiveness against a variety of contaminants outside of MTZ, such as phenol, methylene blue (MB), and humic acid, under comparable photo-Fenton conditions revealed how versatile it is. The nanostructure demonstrated its broad-spectrum catalytic activity by achieving degradation efficiencies of 87% for phenol, 94% for MB, and 80% for humic acid in 60 minutes. Photocurrent measurements and UV-vis diffuse reflection spectroscopy (UV-vis DRS) confirmed that the carbon layer's improved visible-light collecting and the Z-scheme heterojunction's effective charge separation are responsible for this adaptability. The measurements demonstrated consistent performance across pH ranges of 3.0 to 7.0 (adjusted with HCl and Tris-HCl buffer). EPR analysis using 5,5-dimethyl-1-pyrroline-1-oxide (DMPO) confirmed the nanostructure's versatility in activating H_2O_2 and generating reactive oxygen species (ROS) like •OH. Real-time infrared thermal imaging revealed a stable photothermal effect (10-12°C increase) across these pollutants.

Comparative tests with the uncoated FeO_3/MoS_2 composite showed a 10-15% decrease in efficiency for secondary pollutants and a 10% increase in efficiency loss after three cycles, underscoring the dual function of the carbon covering in preserving structural integrity and expanding application. A promising candidate for a variety of environmental remediation scenarios, the nanostructure's versatility was reinforced by its ability to function under varying light intensities (50-100 mW/cm2) and its resistance to agglomeration, as seen in transmission electron microscopy (TEM) images after recycling. These results validate the promise of the $FeO_3/MoS_2@C$ nanostructure as a robust and versatile photocatalyst for tackling various pollution issues.

CONCLUSIONS

Using a straightforward yet creative nanostructure design, the study effectively illustrates the creation of a highly efficient photocatalytic device for environmental cleanup. Synthesized using a simple deposition and carbon-coating process, the $Fe_2O_3/MoS_2@C$ nanostructure demonstrated excellent photo-Fenton performance, outperforming individual Fe_2O_3, MoS_2, and uncoated Fe_2O_3/MoS_2 composites by 92% in 60 minutes with a pseudo-first-order rate constant of 0.038 min^{-1}. Strong visible-light absorption (up to 600 nm), effective charge separation, and robust generation of reactive oxygen species (ROS), especially •OH radicals, were all made possible by the integration of a Z-scheme heterojunction, which was strengthened by oxygen vacancies and a protective carbon layer. These results were verified by EPR and radical trapping experiments.

The exceptional recyclability and adaptability of the nanostructure further confirmed its practical application. The $Fe_2O_3/MoS_2@C$ system demonstrated stability by retaining 88% of its initial activity after five cycles with minimal metal leaching (0.6 ppm Fe, 0.4 ppm Mo). Its broad-spectrum potential was demonstrated by its capacity to degrade a variety of pollutants, including phenol (87%), methylene blue (94%), and humic acid (80%), under different pH and light conditions. The higher charge transfer efficiency (photocurrent density of 0.45 mA/cm^2 and EIS arc radius of 150 Ω) and photothermal effect, which may raise the surface temperature by up to 12°C, further highlight the complementary advantages of the carbon coating and heterojunction design.

In addition to giving a viable foundation for the advancement of photo-Fenton technologies in tackling persistent organic pollutants and promoting sustainable environmental solutions, our results give important insights into the preparation process and structure-function correlations.

REFERENCES

[1] J. Bain and S. S. Staniland, "Bioinspired nanoreactors for the biomineralisation of metallic-based nanoparticles for nanomedicine," *Phys. Chem. Chem. Phys.*, vol. 17, no. 24, pp. 15508–15521, 2015, doi: 10.1039/C5CP00375J.

[2] L. Jia, C. Wang, H. Liu, R. Chen, and K. Wu, "Preparation of Defect-Enriched (Sio32-, Cu2+) – A-Fe2o3/Mos2 Z-Scheme Composites with Enhanced Photocatalytic-Fenton Performance," *SSRN Journal*, 2022, doi: 10.2139/ssrn.4093961.

[3] L. Jia, C. Wang, H. Liu, R. Chen, and K. Wu, "Preparation of defect-enriched (SiO32-, Cu2+) –α-Fe2O3/MoS2 Z-scheme composites with enhanced photocatalytic-Fenton performance," *Journal of Alloys and Compounds*, vol. 923, p. 166293, Nov. 2022, doi: 10.1016/j.jallcom.2022.166293.

[4] M. Verma and A. K. Haritash, "Review of advanced oxidation processes (AOPs) for treatment of pharmaceutical wastewater," *Advances in environmental research*, vol. 9, no. 1, pp. 1–17, Mar. 2020, doi: 10.12989/AER.2020.9.1.001.

[5] B. Sultana, M. G. Hussain, and M. Rahman, "BanSpEmo: a Bangla audio dataset for speech emotion recognition and its baseline evaluation," *IJEECS*, vol. 37, no. 3, p. 2044, Mar. 2025, doi: 10.11591/ijeecs.v37.i3.pp2044-2057.

[6] S. Feijoo, X. Yu, M. Kamali, L. Appels, and R. Dewil, "Generation of oxidative radicals by advanced oxidation processes (AOPs) in wastewater treatment: a mechanistic, environmental and economic review," *Rev Environ Sci Biotechnol*, vol. 22, no. 1, pp. 205–248, Mar. 2023, doi: 10.1007/s11157-023-09645-4.

[7] J. Carbajo, J. E. Silveira, G. Pliego, J. A. Zazo, and J. A. Casas, "Increasing Photo-Fenton process Efficiency: The effect of high temperatures," *Separation and Purification Technology*, vol. 271, p. 118876, Sep. 2021, doi: 10.1016/j.seppur.2021.118876.

[8] [8] C. J. Miller, S. Wadley, and T. D. Waite, "Fenton, photo-Fenton and Fenton-like processes," *Water Intell Online*, vol. 16, pp. 297–332, May 2017, doi: 10.2166/9781780407197_0297.

[9] V. Kavitha and K. Palanivelu, "Degradation of nitrophenols by Fenton and photo-Fenton processes," *Journal of Photochemistry and Photobiology A: Chemistry*, vol. 170, no. 1, pp. 83–95, Feb. 2005, doi: 10.1016/j.jphotochem.2004.08.003.

[10] F. Audino, G. Campanyà, M. Pérez-Moya, A. Espuña, and M. Graells, "Systematic optimization approach for the efficient management of the photo-Fenton treatment process," *Science of The Total Environment*, vol. 646, pp. 902–913, Jan. 2019, doi: 10.1016/j.scitotenv.2018.07.057.

[11] S. A. Hasan *et al.*, "Classification of Multi-Labeled Text Articles with Reuters Dataset using SVM," in *2022 International Conference on Science and Technology (ICOSTECH)*, Batam City, Indonesia: IEEE, Feb. 2022, pp. 01–05. doi: 10.1109/ICOSTECH54296.2022.9829153.

[12] L. K. Sharma and R. Naik, "Saline Wetland Ecosystems," in *Conservation of Saline Wetland Ecosystems*, Singapore: Springer Nature Singapore, 2024, pp. 33–75. doi: 10.1007/978-981-97-5069-6_2.

[13] X. Deng *et al.*, "A nanoreactor with Z-scheme FeS2/MoS2 heterojunctions encapsulated inside the carbon capsule: Insight on preparation method and enhanced performance in photo-Fenton reaction," *Chemical Engineering Journal*, vol. 450, p. 138221, Dec. 2022, doi: 10.1016/j.cej.2022.138221.

[14] M. Che and E. Giamello, "Chapter 5 Electron Paramagnetic Resonance," in *Studies in Surface Science and Catalysis*, vol. 57, Elsevier, 1990, pp. B265–B332. doi: 10.1016/S0167-2991(08)61516-5.

[15] M. Wu *et al.*, "Cascading H2O2 photosynthesis and Fenton reaction for self-sufficient photo-Fenton reactions: A review of recent advances," *Chemical Engineering Journal*, vol. 489, p. 151091, Jun. 2024, doi: 10.1016/j.cej.2024.151091.

[16] M. G. Hussain, M. Rahman, B. Sultana, A. Khatun, and S. A. Hasan, "Classification of Bangla Alphabets Phoneme based on Audio Features using MLPC & SVM," in *2021 International Conference on Automation, Control and Mechatronics for Industry 4.0 (ACMI)*, Rajshahi, Bangladesh: IEEE, Jul. 2021, pp. 1–5. doi: 10.1109/ACMI53878.2021.9528088.

[17] I.-S. Park *et al.*, "In-situ Monitoring System Equipped with FT-IR and QMS and Thermal Decomposition of Zr(NCH$_3$ C$_2$ H$_5$)$_4$ Precursor," *ECS Trans.*, vol. 75, no. 6, pp. 123–128, Aug. 2016, doi: 10.1149/07506.0123ecst.

[18] G. L. Kearns, "The Application of Small Area Electron Spectroscopy for Chemical Analysis (ESCA)," presented at the 1983 Cambridge Symposium, R. S. Bauer and F. H. Pollak, Eds., Cambridge, May 1984, pp. 156–159. doi: 10.1117/12.939300.

[19] M. Saberi and P. Rouhi, "Extension of the Brunauer-Emmett-Teller (BET) model for sorption of gas mixtures on the solid substances," *Fluid Phase Equilibria*, vol. 534, p. 112968, Apr. 2021, doi: 10.1016/j.fluid.2021.112968.